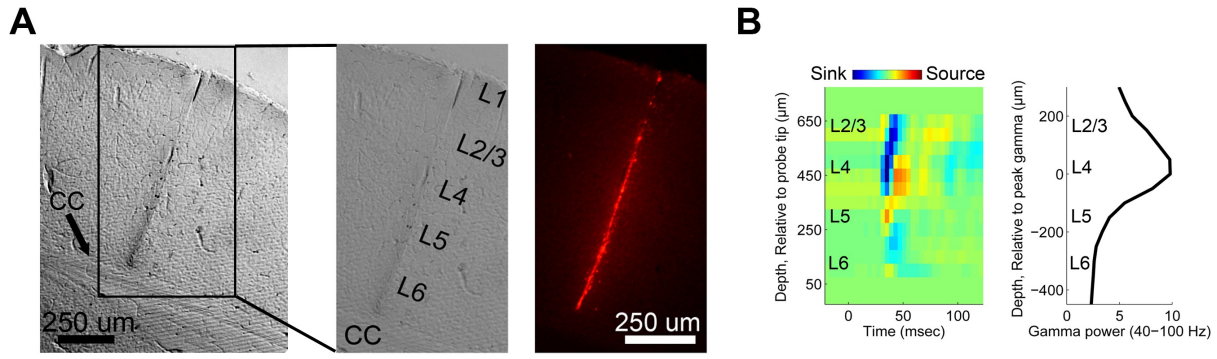

Figure S1. Technique for verifying recording depth. Related to Experimental Procedures. A. Left, Representative histology depicting track of laminar probe in V1, with probe tip reaching the corpus callosum (CC). Right, DiI (applied to probe prior to implant) was used to confirm probe location. **B.** Left, current source density of V1 evoked response to light flashes (depth relative to probe tip). Right, gamma power during spontaneous wake recording prior to stimulation (depth relative to gamma peak) from a representative animal. The earliest sink after visual stimulation occurs in L4 and reliably corresponds to the channels in which gamma power peaked.

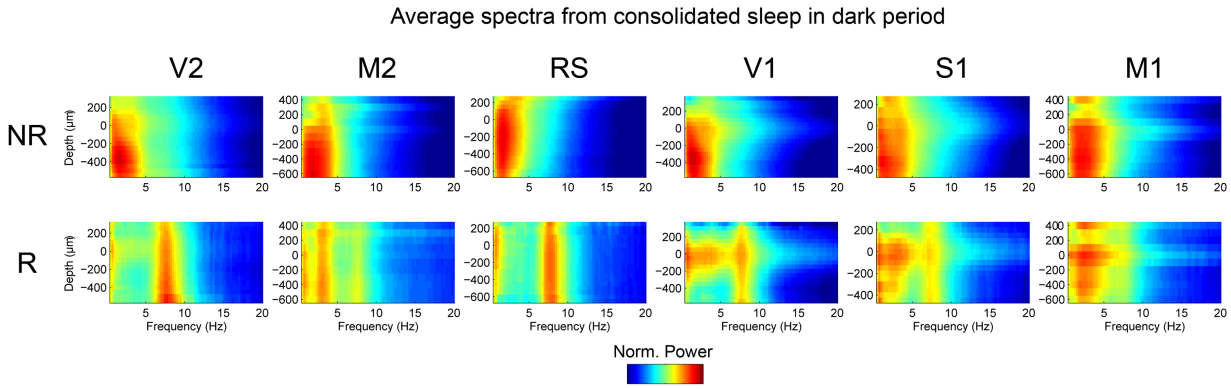

Figure S2. REM SWA occurs in primary cortical areas during the dark period. Related to Figure 2. A, Group spectrograms from consolidated sleep in the dark period in V2 (n=4 mice), M2 (n=4), RS (n=4), V1 (n=11), S1 (n=3) and M1 (n=6) are similar to those from the light period (Figure 2B), ruling out an influence of light or circadian factors on REM SWA. LFP power was normalized by dividing the power in each frequency bin on each channel by the total power across all frequencies and channels on the 16-channel probe. Zero indicates the depth at which the gamma peak occurs, and superficial and deep layers correspond to depths ≥ 100 um and ≤ -100 um, respectively (see Supplemental Experimental Procedures and Figure S1 for details).

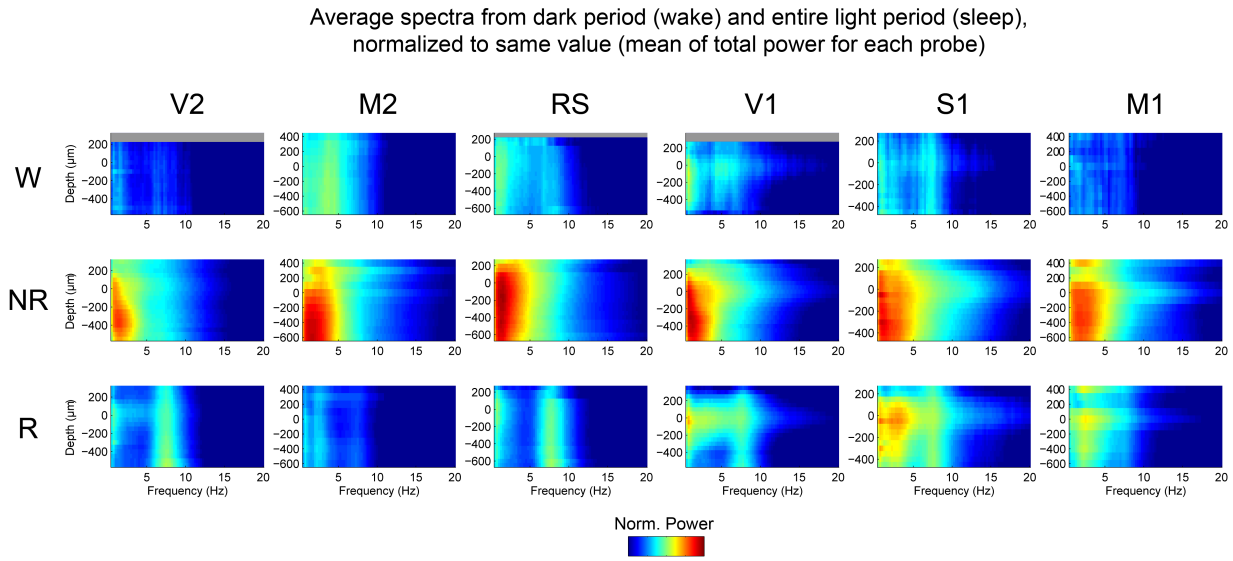

Figure S3. Normalizing all spectra to the same value shows that SWA is greatest in NREM sleep but still present in primary cortical areas in REM sleep. Related to Figure 2. A, Group spectrograms in V2 (W=2 mice, sleep=4 mice), M2 (W=3, sleep=4), RS (W=3, sleep=4), V1 (W=5, sleep=11), S1 (W=1, sleep=3) and M1 (W=2, sleep=6), showing same data as in Figure 2B but using a different normalization method. In this case, the total power in NREM sleep was calculated for each probe, and the mean total NREM power across all probes was used to normalize the power in all states for each probe. This facilitates the comparison of overall power across states and cortical regions. SWA is highest in all areas in NREM sleep and is present during REM sleep in primary cortical areas. Zero indicates the depth at which the gamma peak occurs, and superficial and deep layers correspond to depths ≥ 100 um and ≤ -100 um, respectively (see Supplemental Experimental Procedures and Figure S1 for details). Grey bars indicate layers/depths from which recordings were not available (usually layer 1).

Supplemental Experimental Procedures

Surgery. Under isoflurane anesthesia (2% induction; 1-1.5% maintenance), adult male C57/B6 mice (Jackson Laboratory) were implanted with electrodes for monitoring brain and muscular activity in sterile conditions. Gold screws for recording electroencephalography (EEG) were fixed in burr holes above frontal and/or parietal cortex and screws serving as reference and ground were fixed above the cerebellum and olfactory bulbs, respectively. Target cortical regions were exposed by performing a craniotomy, with underlying dura remaining intact. Laminar silicon probes (NeuroNexus, A1x16, 50 or 100 um site spacing) were inserted perpendicularly to the brain into target cortical regions, including V1 (n=11 mice), V2 (n=4), M1 (n=6), M2 (n=4), S1 (n=3) and/or RS (n=4) using coordinates determined by atlas [S1]. The D/V dimension was adjusted during surgery such that the top contact was placed at the cortical surface (100um-spaced probes) or just below the surface of the brain (50um spaced-probes). Probes were coated with DiI (DilC18(3), Invitrogen) prior to surgery to facilitate histological verification of probe location [S2]. The craniotomy and probe were covered with two-component silicon (QuikSil), followed by dental acrylic (Fusio) to secure the array. A pair of custom-made electromyogram (EMG) cables were implanted bilaterally in the dorsal neck musculature and in the vibrissal musculature. Each animal was implanted with two depth probes, and due to spatial constraints, in most cases these probes had to be placed in opposite hemispheres. Because this arrangement typically left room for an EEG in each hemisphere, most mice had both an EEG and a depth probe in each hemisphere. Animals with probes in M2 were previously injected (>3 weeks prior to electrode implantation) with adeno-associated virus (0.5-2µL) encoding either optogenetic receptors, in ventromedial thalamus (n=2), or pharmacogenetic receptors, in nearby M2 (n=2), using an intrabrain cannula (33GA, Plastics One). In all cases, the baseline sleep recordings used in this study were performed prior to experiments in which the optogenetic/pharmacogenetic receptors were activated. Inspection of raw data and state-specific spectral analysis confirmed that M2 data from mice injected in M2 and from those injected in the thalamus did not differ from each other (data not shown), indicating that the local expression of virus in the former group did not affect M2 activity.

Data from both groups were thus combined. All animal procedures followed the National Institutes of Health Guide for the Care and Use of Laboratory Animals and facilities were reviewed and approved by the IACUC of the University of Wisconsin-Madison, and were inspected and accredited by AAALAC.

Chronic sleep recordings and sleep scoring. Chronic 24-hour recordings commenced at least 7 days after surgery. Local field potentials (LFP; sampled at 256 Hz, band pass filtered from 0.1-100 Hz), multiunit activity (MUA; 25 kHz, 300-5000 Hz), EEG (256 Hz, 0.1-100 Hz) and EMG (256 Hz, 10-100 Hz) were acquired using a PZ amplifier and RZ2 system (Tucker-Davis Technologies). For MUA data, a voltage threshold was manually set based on visual inspection and time stamps and waveforms (46 peri-threshold crossing samples) were acquired for each supra-threshold event. MUA refers to the time stamps associated with all threshold crossings. Sleep stages were manually scored off-line by visual inspection of 4-sec epochs, using a graphic interface (SleepSign, Kissei Comtec), where the EEG, LFP (one superficial and one deep channel from each implanted cortical site), and EMG are displayed simultaneously. Scorers were not blind to the source of each signal and when some signals conflicted, for instance in quiet wake and REM sleep when slow waves occurred in some LFP signals, behavioral state was determined based on the global signals (EEG/EMG). Wake was characterized by high EMG content and low amplitude, high frequency EEG/LFP activity, NREM sleep by low EMG content, and high amplitude, low frequency EEG/LFP activity, and REM sleep by low EMG activity with occasional twitches and strong theta (6-9 Hz) activity in EEG/LFP in all channels except those in middle/superficial layers of primary cortical areas. Simultaneous recordings from primary and secondary/association areas confirmed that slow waves in REM sleep only occurred in middle/superficial channels of primary areas.

Mice are nocturnal and exhibit polyphasic sleep, with many short bouts of sleep interspersed with occasional long bouts [S3,S4]. As expected, mice in this study also slept mainly during the day, often in short sleep bouts, and showed long periods of active wake mainly at night. Percentage of sleep and wake (mean ± SD) during baseline were as follows: light phase, wake = 40.5 ± 4.9%; NREM sleep = 51.6 ± 4.5%; REM sleep = 7.9 ± 1.0%; dark phase, wake = 66.0 ± 5.6%; NREM sleep = 30.7 ± 4.7%; REM sleep = 3.3 ± 1.01%. Mean episode duration was 61.1 ± 19.7 s for wake (range: 4-19516 s), 49.0 ± 11.5 s for NREM sleep (range: 4-752 s), and 58 ± 8.4 s for REM sleep (range: 4-224 s).

Determination of recording site and depth. Mice were transcardially perfused under deep anesthesia (3% isoflurane in oxygen) with 4% paraformaldehyde (PFA) with a 24-h post-fix in PFA. Brains were subsequently sectioned with a vibratome (Leica) into 50um thick sections. Recording location was confirmed histologically. Recording depth was estimated functionally in vivo and confirmed anatomically after perfusion. In all mice the two methods gave consistent results. Histological analysis found that the tips of all laminar probes were either in the corpus callosum or in the bottom of L6 and the laminar location of each site was then calculated based on site spacing using the Allen Brain Atlas as a reference (Suppl. Figure 1A). Functional markers used to estimate recording depth were based on the observation that both multiunit activity and spectral activity in the gamma range (40-100 Hz) varied with depth. Specifically, the firing rates of channels located in superficial and deep layers were overall low and high, respectively (data not shown), consistent with previous reports during wake or under anesthesia [S5,S6]. LFP gamma power also varied across layers in a consistent way: gamma activity generally peaked 450-500um from the tip of the probe in V1 and 1000um from the tip in M1, as determined by electrode spacing. Based on the Allen Brain Atlas, this indicates that the gamma peak occurred in L4 in V1 and at the L3/L5A border in M1. We further verified this relationship in V1 using visual stimulation: the earliest latency sink, known to occur in L4 [S7], occurred at the same depth as the gamma peak (Suppl. Figure 1B). Similar findings were obtained in V2 (not shown). Gamma peaks consistent with histology were also present in S1, M2, and RS. To correct for slight differences in implant depth across mice, we set the depth of the channel with the gamma peak as "0" and assigned each channel a depth relative to this site. To be consistent across animals with 50 um and 100 um spacing, sites in the deep layers (L5-6) were always defined as starting at -100 um, i.e. 100 um below the "zero depth" defined as the site where the gamma peak occurs (putative L4 in sensory cortex, putative bottom of L3 in motor cortex). Middle/superficial layers (L1-4) were considered to be all sites at or above -50um (50 um probes) or 0 um (100 um probes). Indeed, in mice with 50um probes, gamma values were often similar between sites at 0 and -50um, with a sharp drop occurring between -50um and -100um.

State-specific spectral analysis. All electrophysiological data were analyzed using custom Matlab (MathWorks) scripts. Spectral analysis was performed in 4-sec epochs using the fast Fourier transform using FieldTrip [S8] scripts implemented in Matlab. In order to study state-specific activity patterns and avoid mixed transitional states and brief bouts of sleep or wake we focused on the 12-h light phase, when mice sleep more, and only considered consolidated

bouts of NREM sleep (>2 min, without wake interruptions > 4 sec) and REM sleep (>40 sec, with no wake interruptions). For REM sleep analysis, we further excluded the first 20 sec of each REM episode in order to avoid transitions from NREM sleep, which may represent a distinct in-between state [S9]. We also excluded the final 4 sec of each REM bout before the transition to wake. To confirm accurate state detection, we performed spectral analysis of sleep EEG data from frontal and parietal cortex and found the expected peak in low frequencies (<4 Hz) in NREM sleep and in theta range (6-9 Hz) in REM sleep (Figure 1C).

To study differences between active wake, when mice actively explore, and quiet wake, we identified consolidated periods of wake in the light cycle (relatively rich in quiet wake) and in the dark cycle (relatively rich in active wake). For wake in the light period, we identified consolidated wake episodes lasting at least 10 min. For wake in the dark period, we identified the longest bout of wake after lights off and, if shorter than an hour, added other periods of at least 20 min of consolidated wake in order to acquire at least 1 hour worth of data. Overall, this approach ensured that the wake data had minimal transitional epochs, which may contain sleep-like features. Wake epochs were then further subdivided into active and quiet wake based on whether their EMG content was in the top 33 percentile or bottom 33 percentile of wake EMG activity calculated for the entire 24-h baseline. LFP recordings for all wake epochs were visually inspected to identify epochs without movement artifacts. Data from active and quiet wake were only included in group analysis if at least 3 min of clean data were obtained.

To investigate differences in SWA between phasic and tonic REM sleep, we automatically detected phasic whisking events in the vibrissal EMG using a custom algorithm. Next, spectral activity from epochs in which at least 25% of the 4-sec epoch was occupied by whisking activity ("phasic REM") was compared to spectral activity from epochs in which less than 25% of the epoch contained whisking activity ("tonic REM").

Slow wave detection and analysis of underlying neuronal dynamics. Slow waves were detected from LFP recordings using a previously described method [S10]. Briefly, LFPs were bandpass filtered from 0.5 to 4 Hz, then local maxima were automatically detected. For each mouse, the LFP channels with maximum NREM slow wave activity (SWA) and REM SWA were used to detect slow waves in each state. For analysis of the currents and MUA associated with individual slow waves, slow waves with maximum amplitudes in the top 33 percentile were used.

Current source density (CSD) analysis was performed using scripts from CSDPlotter toolbox [S11], using the standard method for calculating the second spatial derivative:

$$\frac{\partial^2 \varnothing}{\partial z^2} = \frac{\varnothing\,(z + n \cdot h) - 2\varnothing(z) + \varnothing(z - n \cdot h)}{(n \cdot h)^2}$$

where Ø is the local field potential, z is the recording site, h is the spacing between sites (either 50 um or 100 um), and n is the number of sites between z and the site used to calculate the CSD. For all CSD calculations, the product of n and h was 100 um. For probes with 50 um spacing, LFPs two sites away from each site were used. For analysis of MUA locked to slow waves, MUA from -1 to +1 s, relative to the peak of the slow wave, was isolated. Firing rate for this period was normalized to the baseline firing rate, defined as -1 to -0.5 s prior to the peak of the slow wave.

For analysis of homeostatic regulation of specific slow wave parameters, slow waves detected in one of the two compartments (superficial, deep) were removed if a slow wave of higher amplitude was simultaneously present in the other compartment, because this was taken as a sign that the slow wave originated in the other compartment. Slow waves were divided into quintiles, and slow waves in the top quintile were used. A paired-sample t-test was used for statistical comparison of slow wave parameters at different time points.

Supplemental References

S1. Franklin, K., and Paxinos, G. (2008). The Mouse Brain in Stereotaxic Coordinates, (Academic Press).

S2. Magill, P.J., Pogosyan, A., Sharott, A., Csicsvari, J., Bolam, J.P., and Brown, P. (2006). Changes in functional connectivity within the rat striatopallidal axis during global brain activation in vivo. J Neurosci *26*, 6318-6329.

S3. McShane, B.B., Galante, R.J., Jensen, S.T., Naidoo, N., Pack, A.I., and Wyner, A. (2010). Characterization of the bout durations of sleep and wakefulness. J Neurosci Methods *193*, 321-333.

S4. Douglas, C.L., Vyazovskiy, V., Southard, T., Chiu, S.Y., Messing, A., Tononi, G., and Cirelli, C. (2007). Sleep in Kcna2 knockout mice. BMC biology *5*, 42.

S5. Sakata, S., and Harris, K.D. (2012). Laminar-dependent effects of cortical state on auditory cortical spontaneous activity. Front Neural Circuits *6*, 109.

S6. Sakata, S., and Harris, K.D. (2009). Laminar structure of spontaneous and sensory-evoked population activity in auditory cortex. Neuron *64*, 404-418.

S7. Niell, C.M., and Stryker, M.P. (2008). Highly selective receptive fields in mouse visual cortex. The Journal of neuroscience : the official journal of the Society for Neuroscience *28*, 7520-7536.
S8. Oostenveld, R., Fries, P., Maris, E., and Schoffelen, J.M. (2011). FieldTrip: Open source software for advanced analysis of MEG, EEG, and invasive electrophysiological data. Comput Intell Neurosci *2011*, 156869.
S9. Gottesmann, C. (1996). The transition from slow-wave sleep to paradoxical sleep: evolving facts and concepts of the neurophysiological processes underlying the intermediate stage of sleep. Neuroscience and biobehavioral reviews *20*, 367-387.
S10. Vyazovskiy, V., Riedner, B.A., Cirelli, C., and Tononi, G. (2007). Sleep homeostasis and cortical synchronization: II. A local field potential study of sleep slow waves in the rat. Sleep *30*, 1631-1642.
S11. Pettersen, K.H., Devor, A., Ulbert, I., Dale, A.M., and Einevoll, G.T. (2006). Current-source density estimation based on inversion of electrostatic forward solution: effects of finite extent of neuronal activity and conductivity discontinuities. J Neurosci Methods *154*, 116-133.